Quantifying APD–ARI Differences Across Endo-Epicardial Surfaces in Human and Porcine Hearts

Jimena Siles[1,3], Casey Lee-Trimble[3], Evan Rheaume[3],Shahriar Iravanian[4], Flavio Fenton[3], João Salinet[1], Ilija Uzelac[2]

[1]HEartLab, Federal University of ABC, São Bernardo do Campo, Brazil
[2]School of Medicine, Virginia Commonwealth University, Richmond, VA, USA
[3]School of Physics, Georgia Institute of Technology, Atlanta, GA, USA
[4]Emory University, Atlanta, GA, USA

Abstract

This study compares activation–recovery interval (ARI) from unipolar electrograms with optically derived action potential duration (APD) as the reference, across endocardial and epicardial surfaces in healthy porcine (N=3) and pathological human hearts (N=2). Optical and electrical signals were recorded simultaneously using high-speed cameras and transparent electrode arrays. APD was computed at 70–90% repolarization (APD_{70}, APD_{80}, APD_{90}), while ARI was measured by Wyatt and alternative methods. Comparisons revealed layer-dependent differences: in pigs, the Wyatt method showed the best agreement with endocardial APD, whereas the alternative method better matched epicardial APD; in humans, the alternative method yielded the closest agreement with APD_{90} in the endocardium and with APD_{80} in the epicardium. These findings highlight the need for surface-specific approaches when estimating repolarization from electrical recordings.

1. Introduction

Worldwide, one in three people will develop a potentially life-threatening cardiac rhythm disorder during their lifetime. From these cardiac arrhythmias, ventricular fibrillation is the most common cause of sudden death, accounting for about 80% of cases [1]. Dynamic alternation in cardiac repolarization play a central role in the generation of spatiotemporal gradients [2] and mechanisms such as reentry or triggered activity. Its characterization, through metrics such as action potential duration (APD) and activation–recovery interval (ARI), enables the identification of risk patterns [3], optimization of therapeutic strategies, and improved interpretation of arrhythmic mechanisms in both experimental and clinical settings. In conventional electrophysiological studies commonly used in clinical settings, factors such as electrode polarity, placement, and limited spatial resolution can introduce errors in repolarization assessment [4]. In contrast, optical mapping provides a direct measurement of transmembrane voltage with high spatial and temporal resolution, independent of electrode orientation or polarity, enabling a more precise characterization of repolarization patterns [5].

This study aims to evaluate the proximity between repolarization results recorded simultaneously in the endocardium and epicardium using electrical contact mapping and optical mapping. On the electrical side, the Wyatt and alternative methods [4] were applied to calculate repolarization intervals from unipolar electrograms. These intervals were compared with APD values at 70%, 80%, and 90% repolarization [5]. Beyond this dual-layer approach, a translational comparison was also performed between healthy porcine and pathological human hearts. By employing optical mapping as the reference for transmural data acquired in pigs and humans, this work enhances the interpretation of electrical measurements.

2. Methods

2.1. Heart Extraction and Right Ventricular Free Wall Preparation

Three female pigs (P1, P2, P3) were donated by a surgical training facility right after euthanasia, as described in previous studies [6]. Euthanasia was performed using a pentobarbital and phenytoin solution. The hearts were quickly excised via left lateral thoracotomy and perfused with Tyrode's solution containing adrenaline and heparin, followed by cold cardioplegia for transportation. The human hearts used in this study were provided by the VCU Heart Transplant Program under an approved Institutional Review Board (IRB) protocol (HM11452; H1 and H2).

Hearts were surgically extracted by the cardiac surgery team during transplantation and perfused with cardioplegia for transportation. The right ventricle was separated and prepared in a free wall configuration to allow simultaneous imaging of the epicardium and endocardium. The heart preparation was perfused with Tyrode's solution, followed by administration of the JPW-6003 V_m dye and blebbistatin.

2.2. Setup Implementation

The setup consists of two main systems: an optical mapping as in [2] combined with an multielectrode arrays (MEAs), as shown in Figure 1. For MEA customization, 16 platinum electrodes (1 × 1 mm), obtained from the Livewire Duo-Decapolar catheter (St. Jude Medical/Abbott), were fixed onto a transparent acetate base and arranged in a 4 × 4 grid with an inter-electrode spacing of 1 cm. A reference electrode was positioned at a distal location from the MEAs (Figure 1, left). For pig experiments, two EMCCD cameras (Evolve 128, Photometrics) were used, whereas for human experiments, two CMOS cameras (DMK 37BUX287, Pregius) were employed. In both cases, one camera was oriented toward the endocardium and the other, via a mirror, toward the epicardium (Figure 1, right). Six LEDs (650–660 nm) with corresponding optical filters illuminated the tissue. Additionally, the setup includes an electrical-optical synchronization and stimulation system. For this analysis, a pacing cycle length (PCL) of 800 ms was applied to both pig and human hearts.

2.3. Signal Pre-Processing

Electrical recordings were first symmetrically padded and then filtered using a second-order Butterworth bandpass IIR filter to remove both low and high frequency noise (0.5 and 200 Hz, respectively). User-defined IIR notch filters were subsequently applied to remove specific frequency components, such as 60 Hz powerline interference, with a quality factor of 30 [7]. For optical recordings, the acquired 3D array was filtered using an adaptive one-dimensional Gaussian filter applied to each temporal trace within the three-dimensional optical mapping dataset and an adaptive Gaussian smoothing filter applied to each frame or two-dimensional spatial map. No resampling was applied across datasets with different sampling frequencies. Instead, all parameters were extracted at native temporal resolution and compared in milliseconds, as recommended in previous studies [8].

2.4. Repolarization Analysis

The Local activation time (LAT) for electrical recordings was defined as the maximum down-slope of the unipolar electrograms [9]. In the case of optical recordings, LAT was considered as the time point at which the signal crossed the 50% level between its minimum and maximum values (Fig. 1, bottom, horizontal gray dotted line). To improve temporal resolution beyond the native 2 ms sampling interval (500 Hz), a local linear regression (polyfit) was applied around the 50% crossing point (Fig. 1, blue) [5]. APD for optical recordings was defined as the interval between LAT and the time point at which the signal decayed to a specified percentage of its maximal amplitude: 70% (APD_{70}), 80% (APD_{80}), and 90% (APD_{90}) as is presented in Figure 1 as orange dotted lines. The ARI, derived from unipolar electrograms, was defined as the time between LAT and recovery time (RT). Two methods were used to determine RT: the Wyatt and the alternative method [4]. The ARI_W identifies RT at the steepest upslope of the T-wave, whereas the ARI_A identifies RT at the steepest downslope for positive T-waves and at the steepest upslope for negative T-waves (Fig. 1, bottom).

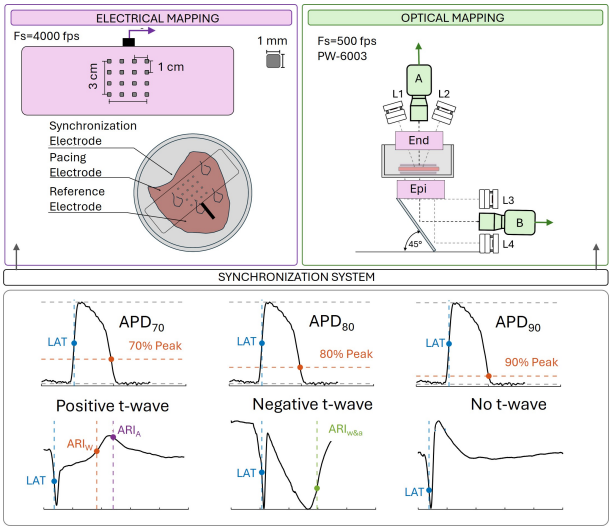

Figure 1. Experimental setup and repolarization analysis. Top: Electrical and optical mapping systems. Bottom: Representative APD at 70%, 80%, and 90% of repolarization. ARI for a positive t-wave using the Wyatt (ARI_W) and alternative methods (ARI_A), negative t-wave, where $ARI_{w\&a}$ is the same for both methods and no t-wave.

3. Statistical Analysis

Comparison matrices were generated using ARI and APD values (three consecutive beats) extracted from sixteen predefined sites corresponding to the electrodes of each MEA. ARI_W and ARI_A were compared with APD_{70}, APD_{80}, and APD_{90}, and analyses were performed independently for endocardial and epicardial surfaces. To characterize the data distribution, we applied

a median and interquartile range (IQR) analysis, reporting central tendency and dispersion as median [Q1-Q3]. The proximity between optical and electrical repolarization metrics was assessed using the absolute difference between APD and ARI, expressed as $|APD - ARI|$. This parameter quantifies the level of agreement between the two measures at each recording site, high proximity ($|APD - ARI|$ close to 0 ms) indicates that ARI reliably tracks the repolarization behavior measured optically, while low proximity ($|APD - ARI| \geq$ 20–30 ms) highlights potential limitations in the use of ARI as a surrogate for action potential duration.

4. Results

Figure 2 shows representative examples of the epicardial and endocardial surfaces of pig and human hearts, respectively. Porcine hearts had average dimensions of 11.7×9.5 cm (SD = 0.3 and 0.5 cm, respectively) and an average weight of 216.9 g (SD = 23.0 g). The human hearts had average dimensions of 17.0×12.7 cm (SD = 1.0 and 0.6 cm, respectively) and an average weight of 556.0 g (SD = 67.7 g). Human hearts exhibited greater adipose tissue thickness and, in some cases, evidence of fibrosis. The final experimental setup is shown in Figure 2 (right), with the ventricular preparation placed inside the imaging chamber and both cameras actively recording. Both the epicardial and endocardial surfaces are shown with their respective MEA positioned in place.

For pigs, repolarization values generally ranged between 250 and 450 ms; however, in P3, ARI_A exceeded 500 ms. According to Figure 3A, ARI_A tended to yield higher values than APD, whereas ARI_W was consistently lower over the endocardium. In P2, epicardial results showed greater variability and represented the only case in which both ARI estimates were lower than the corresponding APD values. Based on the original recordings, only positive T-waves were observed across both surfaces in pigs. For human hearts repolarization values ranged between 300 and 600 ms. As shown in Figure 3B, in H1, exclusively negative T-waves were observed on both surfaces, while in the endocardium of H2 a positive T-wave was detected. For negative waves, $ARI_{w\&a}$ was consistently located between the APD values, irrespective of the cardiac surface.

Analyzing the absolute difference in the porcine endocardium, APD_{70} and ARI_W showed the highest percentages of proximity (values $\leq$ 20 ms) in P1 (98%) and P3 (27%). In contrast, only in P2 was a closer agreement observed between ARI_A and APD_{90}. In the epicardium, the strongest correspondence was found between APD_{70} and APD_{80} with ARI_A (P1 = 73%, P2 = 33%), whereas in P3 the closest proximity was observed between ARI_W and APD_{70} (56%). In human hearts, within the endocardium of H2, ARI_A showed greater proximity to APD_{90} (27%), while in H1, ARI was closer to APD_{70} (31%). In the epicardium, the strongest correspondence was observed between $ARI_{w\&a}$ and APD_{70} in H1 (35%) and with APD_{80} in H2 (60%).

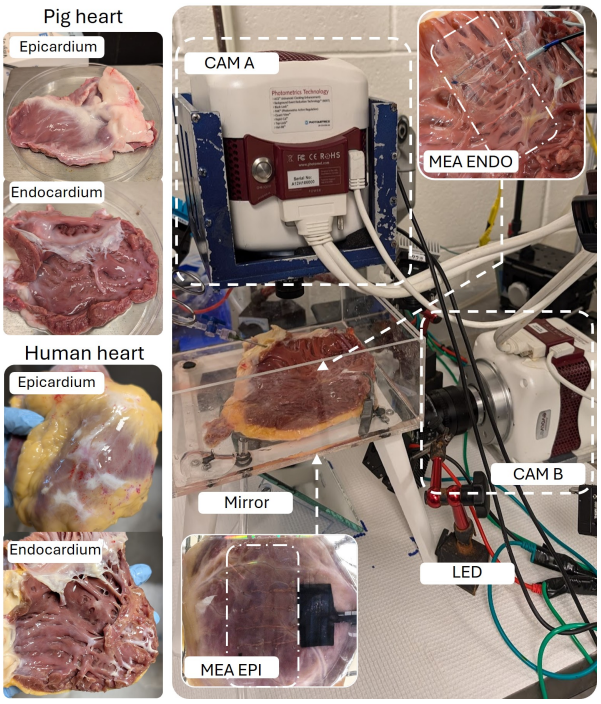

Figure 2. Representative images of porcine and human ventricular preparations showing epicardial and endocardial surfaces, and the dual-camera setup with respective MEAs for simultaneous recordings.

5. Discussion and Conclusion

A dual optical and electrical mapping system was implemented for both porcine and human hearts, enabling the simultaneous acquisition of optical and electrical recordings. This setup allowed for the direct comparison of repolarization metrics across species and cardiac surfaces. Nevertheless, the system presents some limitations. In custom MEAs, factors such as soldering quality and base adhesion introduce variability in the measurements. In addition, reference selection and pacing electrode locations evolved throughout the experiments, potentially affecting data consistency. Furthermore, ARI carries intrinsic limitations as a surrogate for repolarization, since it is influenced by multiple factors, and a perfect agreement with optical APD metrics cannot be expected. In pigs, endocardial APD_{70} and APD_{80} showed better correspondence with ARI_W, whereas in the epicardium APD_{70} and APD_{80} presented smaller differences with ARI_A. Overall, no sin-

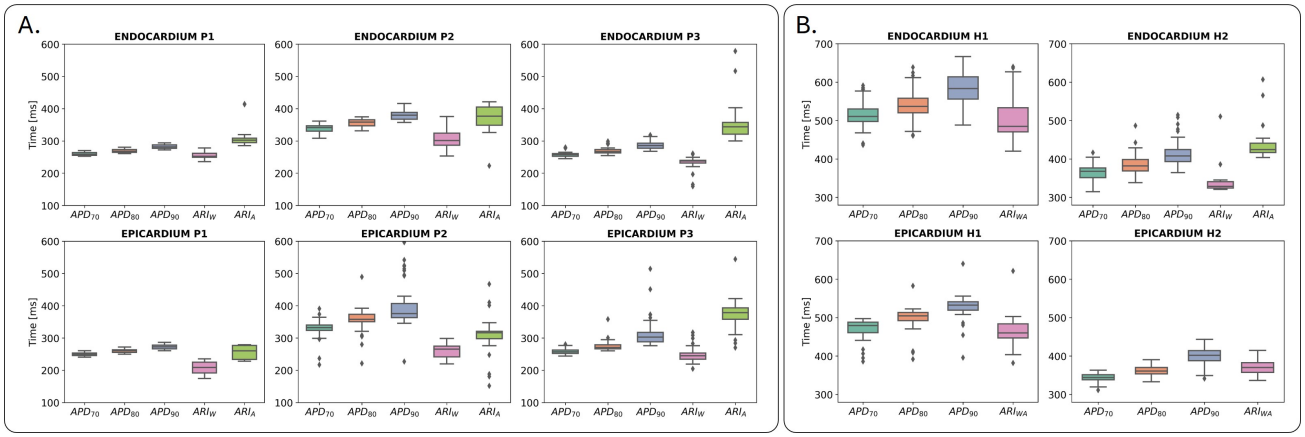

Figure 3. A. Boxplots comparing APD_{70}, APD_{80}, APD_{90}, ARI_W, and ARI_A for endocardial and epicardial surfaces in porcine hearts (P1-P3). B. Equivalent comparison for human hearts (H1-H2). Boxplots display the interquartile range (Q1-Q3), with the horizontal line indicating the median.

gle method consistently outperformed the other. These findings suggest that ARI estimation, particularly in the endocardium, may be influenced by interindividual variability and tissue-specific characteristics, requiring careful consideration when selecting the most appropriate approach. In conclusion, although the implementation of the dual mapping system provided valuable insights into the relationship between optical and electrical repolarization metrics, the results were not conclusive and further refinement methodology is required.

Acknowledgments

This work was supported by FAPESP grants #2020/03601-9, #2023/04822-7, and #2018/25606-2, CNPq INCT INTERAS call 58/2022, NIH grant 2R01HL143450–05A1 and the Dr. Kenneth Ellenbogen Endowment. We thank the VCU surgeons for the explanted human hearts.

References

[1] Wever EF, Robles de Medina EO. Sudden death in patients without structural heart disease. Journal of the American College of Cardiology 2004;43(7):1137–1144.

[2] Gizzi A, Cherry EM, Gilmour Jr RF, Luther S, Filippi S, Fenton FH. Effects of pacing site and stimulation history on alternans dynamics and the development of complex spatiotemporal patterns in cardiac tissue. Frontiers in Physiology 2013;4:71.

[3] Haws CW, Lux RL. Correlation between in vivo transmembrane action potential durations and activation-recovery intervals from electrograms. effects of interventions that alter repolarization time. Circulation 1990;81(1):281–288.

[4] Stoks J, Bear LR, Vijgen J, Dendale P, Peeters R, Volders PG, Cluitmans MJ. Understanding repolarization in the intracardiac unipolar electrogram: a long-lasting controversy revisited. Frontiers in Physiology 2023;14:1158003.

[5] Laughner JI, Ng FS, Sulkin MS, Arthur RM, Efimov IR. Processing and analysis of cardiac optical mapping data obtained with potentiometric dyes. American Journal of Physiology Heart and Circulatory Physiology 2012;303(7):H753–H765.

[6] Uzelac I, Crowley CJ, Iravanian S, Kim TY, Cho HC, Fenton FH. Methodology for cross-talk elimination in simultaneous voltage and calcium optical mapping measurements with semasbestic wavelengths. Frontiers in Physiology 2022; 13:812968.

[7] Starreveld R, Knops P, Roos-Serote M, Kik C, Bogers AJ, Brundel BJ, de Groot NM. The impact of filter settings on morphology of unipolar fibrillation potentials. Journal of Cardiovascular Translational Research 2020;13(6):953–964.

[8] Efimov IR, Cheng Y, Van Wagoner DR, Mazgalev T, Tchou PJ. Virtual electrode–induced phase singularity: A basic mechanism of defibrillation failure. Circulation Research 1998;82(8):918–925.

[9] Cantwell CD, Roney CH, Ng FS, Siggers JH, Sherwin SJ, Peters NS. Techniques for automated local activation time annotation and conduction velocity estimation in cardiac mapping. Computers in Biology and Medicine 2015;65:229–242.

Address for correspondence:

Jimena Gabriela Siles Paredes
Federal University of ABC - UFABC
Street: Av. Anchieta, São Bernardo do Campo - SP, Brazil
E-mail: jimena.gabriela@ufabc.edu.br